Shahrood University of Technology

Journal of Artificial Intelligence and Data Mining (JAIDM)
Journal homepage: http://jad.shahroodut.ac.ir

Research paper

A Phenology Based Paddy Rice Mapping by Correlation Analysis on Sentinel-1/2 Imagery in Fragmented Lands Using GEE Platform

Fateme Namazi[1], Mehdi Ezoji[1]* and Ebadat Ghanbari Parmehr[2]

1. Faculty of Electrical and Computer Engineering, Babol Noshirvani University of Technology, Babol, Iran.
2. Department of Geomatics, Faculty of Civil Engineering, Babol Noshirvani University of Technology, Babol, Iran.

Article Info

Article History:
Received 08 December 2024
Revised 30 January 2025
Accepted 06 March 2025

DOI:10.22044/jadm.2025.15379.2639

Keywords:
Phenology, Sentinel-1/2, Fragmented Farmland, Correlation Analysis, Rice Crop Mapping, Google Earth Engine.

**Corresponding author: m.ezoji@nit.ac.ir (M. Ezoji).*

Abstract

Paddy fields in the north of Iran are highly fragmented, leading to challenges in accurately mapping them using remote sensing techniques. Cloudy weather often degrades image quality or renders images unusable, further complicating monitoring efforts. This paper presents a novel paddy rice mapping method based on phenology, addressing these challenges. The method utilizes time series data from Sentinel-1 and 2 satellites to derive a rice phenology curve. This curve is constructed using the cross ratio (CR) index from Sentinel-1, and the normalized difference vegetation index (NDVI) and land surface water index (LSWI) from Sentinel-2. Unlike existing methods, which often rely on analyzing single-point indices at specific times, this approach examines the entire time series behavior of each pixel. This robust strategy significantly mitigates the impact of cloud cover on classification accuracy. The time series behavior of each pixel is then correlated with this rice phenology curve. The maximum correlation, typically achieved around the 50-day period in the middle of the cultivation season, helps identify potential rice fields. A Support Vector Machine (SVM) classifier with a Radial Basis Function (RBF) kernel is then employed, utilizing the maximum correlation values from all three indices to classify pixels as rice paddy or other land cover types. The implementation results validate the accuracy of this method, achieving an overall accuracy of 99%. All processes were carried out on the Google Earth Engine (GEE) platform.

1. Introduction

Rice is a staple food for over half of the world's population [1] and Asia accounts for more than 90% of rice production [2]. Furthermore, the International Food Policy Research Institute estimates an annual growth in rice demand of 1.8%. This escalating demand underscores the critical need for accurate and timely rice crop mapping. Rice crop mapping is essential for maintaining food security and is closely linked to environmental concerns, including greenhouse gas (CH4) emissions [3] [4], climate change, disease transmission [5] and soil quality improvements and freshwater use on the regional, national and global scales. Consequently, obtaining accurate and timely data on crop distribution and its changes is crucial for ensuring food security and environmental sustainability.

Beyond food security, precise crop mapping plays a key role in agricultural policy-making, resource management, and disaster response. It helps governments and organizations optimize irrigation, predict yield variations, and implement targeted interventions for droughts, floods, and pest outbreaks. Additionally, integrating remote sensing-based crop mapping with machine learning and geospatial analysis improves predictive models, enabling early warnings of potential crop failures and promoting market stability. Traditional human statistics and remote-sensing monitoring are the two most important methods for

determining the rice-planting area. Manual data collection requires field surveys, a process that is time-consuming and expensive. Furthermore, the data update process is slow, significantly hindering its practical use. Traditional survey methods are limited in that they represent rice-planting areas only as tabular data, lacking explicit spatial distribution information. This limitation makes it difficult to visualize or analyze the geographical patterns of rice cultivation. In contrast, remote sensing techniques overcome these challenges by providing an effective and reliable means to map rice paddies, offering detailed spatial distribution insights across regional and global scales. In addition to being cost-effective, this method has higher efficiency and can be used in a broader scope.

Rice mapping methods can be broadly categorized into two approaches: phenology-based methods and spectral learning methods. In methods based on spectral learning, band values or indices extracted from them are directly used for classification with machine learning methods. However, the ability of these algorithms to learn from unprocessed data of bands and indices is limited. To increase learning ability and classification accuracy, deep learning methods were proposed in this field. Classical convolutional networks algorithm was used in [6] and [7], Long short-term memory (LSTM) algorithm in [8] and ConvLSTM algorithm in [9] and [10]. The primary challenge with deep learning techniques is their reliance on extensive training data, which is not available in many areas.

Phenology-based methods derive rice phenology parameters—such as start of season (SOS), end of season (EOS), length of season (LOS), and peak of season (POS)—from time series indices. Classification is done using different methods such as threshold [11], statistical and machine learning such as SVM [12], Random Forest (RF) [13], Decision Tree (DT) [14], etc. Due to rice's distinct phenology, these methods often achieve superior classification results. However, they rely on index values at specific times, making them vulnerable to errors if these values fluctuate abnormally. Such fluctuations can result from factors like cloud-induced low image quality [15], weed interference under certain weather conditions [16], and human activities such as successive plantings, which can shift parameters such as SOS and EOS. This study proposes a phenology-based approach that mitigates these challenges.

Remote sensing datasets, encompassing both optical and synthetic aperture radar (SAR) data, are extensively employed in rice crop mapping [20]. A review by [21] detailed the evolution of these techniques from the 2010s to 2020, classifying methods into three categories: (I) Optical remote sensing-based methods, (II) microwave remote sensing-based methods, and (III) integrated methods combining both optical and microwave data.

Optical remote sensing data, derived from vegetation photosynthetic parameters such as the leaf area index, provide valuable insights into the growth status of crops. Many scholars have demonstrated their superiority in identifying paddy rice [17]. Numerous researchers have engaged in the processes of interpolation, cloud removal, and smoothing when dealing with optical remote sensing data. While these procedures effectively mitigate the impact of cloud noise to a certain degree, it is important to note that they cannot entirely eliminate local noise fundamentally. In other words, despite efforts to address cloud removal, complete elimination of local noise remains a persistent challenge. To tackle this limitation, many studies have used time series data for crop mapping [22].

In subtropical and tropical regions, flooding and transplanting occur during the cloudy and rainy seasons, significantly reducing the availability of time series data. As a result, SAR data are increasingly used in areas with frequent cloud cover and rainfall. Due to the characteristics of active imaging and its long wavelength, it can capture images regardless of the time or weather conditions. But their number of bands is limited and they have less usable information than optical data. Given the complementary information of optical and SAR data, integrating both datasets emerge as the most efficient method for rice crop mapping in cloud-prone regions.

In regions where agricultural lands are fragmented and cropping patterns are complex, the number of pixels located at the boundaries between different land types increases. These mixed pixels, containing two crop types, make it challenging to generate an accurate crop map.

In the previous study[18], two time series indices —NDVI and LSWI—were selected from Sentinel-2 satellite data. The NDVI time series index rises as the plant biomass increases during the initial stages of rice growth, resembling a Gaussian function curve. However, during the later stages, the index value decreases due to changes in the color of the rice plants.

The LSWI index, which detects water, exhibits its highest value during preparation and transplanting, always decreasing during the cultivation period. In that study, after a series of pre-processing, the time

series curves of LSWI and NDVI indices were extracted during the rice cultivation period and considered as rice phenology. To classify each pixel in the satellite images, the similarity between the pixel time series behavior and the rice phenology curve was evaluated using the correlation operator, with the maximum correlation value and its corresponding time of occurrence serving as classification features.

In the present study, to increase the classification accuracy, after examining the various indices of Sentinel-1 images, CR index was extracted and used along with LSWI and NDVI indices. Due to multiple plantings and successive cultivation of different crops in the study area, rice cultivation may be delayed or accelerated. In addition, the transition from the sea coast to the foothills influences rice cultivation timing, resulting in later planting and longer cultivation periods in cooler regions. Therefore, to reduce the effects of these variations, the steps for obtaining the maximum correlation were modified. The time and duration of the period were adjusted to encompass the maximum range of rice planting changes in the region. This modification allows for the assessment of a pixel's phenological behavior across the entire cultivation period, eliminating the reliance on specific time points for classification. Consequently, the classification result is less affected by delays or accelerations in rice cultivation. Google Earth Engine (GEE) offers powerful online and parallel computing capabilities for processing remote sensing data. All processes described in this paper were conducted using GEE platform. The aims of this study are: (1) To accurately extract the rice phenology curve for three indices NDVI, LSWI and CR such that they are suitable for matching; (2) To extract prominent features for classification based on the correlation between time series indices and the extracted phenology curve; (3) To demonstrate the sufficiency of a simple and fast classifier for rice mapping even with a small number of training data; (4) To improve the rice crop mapping by using the combined correlation operator.

2. Study Area and Datasets

2.1. Study Area

Mazandaran Province, located in northern Iran between the Alborz Mountain range and the Caspian Sea (Figure 1), presents a unique environment for rice cultivation. Characterized by a mild and humid climate, the region exhibits several distinctive features: primarily rice cultivation on flooded soils, small paddy fields typically under half a hectare, and dispersed settlements within the agricultural landscape. Moreover, the close proximity of rice paddies to other crop types complicates rice mapping. In fact, frequent cloud cover in the region presents a significant challenge for remote sensing applications, as satellite imagery can be frequently unavailable. Additionally, various rice cultivars are cultivated in the region, with some paddy fields incorporating multi-crop systems, leading to variations in planting and harvesting times.

Early and late rice are the two main groups cultivated in the area. While their growing periods are roughly equal, the late rice variety exhibits higher yields and extends its cultivation cycle slightly longer. In this region, rice cultivation typically lasts 80 to 110 days, with the first 60 to 90 days involving flooding. The spatial distribution of horticultural crops within the region creates a complex and fragmented mosaic of land use. Alongside rice, this includes a range of crops such as citrus, deciduous trees, wheat, and various vegetables. In recent times, as a result of suitable weather conditions, the cultivation of rice twice a year in this region has grown substantially.

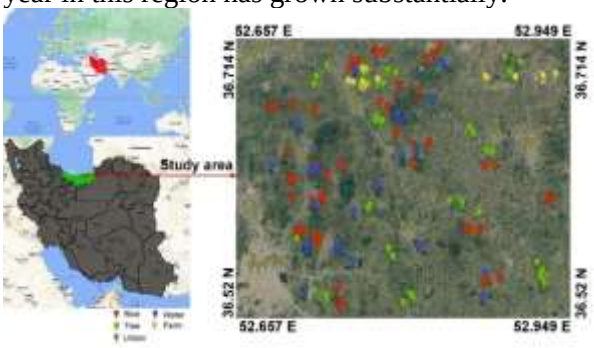

(a) (b)

Figure1. (a) The location of the studied area in the north of Iran (b) Field survey locations.

2.2. Datasets

This study utilizes optical data from Sentinel-2 and microwave data from Sentinel-1. The main features of these datasets are summarized in Table 1.

Table 1. Features of Sentinel 1 and 2 data available in GEE.

Satellite/Property	Sentinel-1	Sentinel-2
Format	IW_GRD	Level-1C
Polarization/Band	VH	13 Spectral bands
Spatial Resolution (m)	10	10-20
Temporal Resolution (d)	6	5
Time span	1 February 2023 to 1 December 2023	

2.2.1 Sentinel-1

Sentinel-1 satellites employ C-band synthetic aperture radar (SAR) technology, enabling data

acquisition under all weather conditions and at any time of day. With their equatorial orbit, Sentinel-1A and 1B revisit the study area every six days. The satellites operate in four data acquisition modes: Interferometric Wide Swath (IW), Strip Map (SM), Extra Wide Swath (EW), and Wave (WV), with IW being the primary operational mode. Within IW mode, imagery is captured in two polarization configurations: VV (vertical transmit and vertical receive) and VH (vertical transmit and horizontal receive). Notably, VH polarization is more sensitive to flood signals than VV polarization [11]. This study utilizes Sentinel-1A Ground-Range-Detected (GRD) VH and VV images. Figure 2 shows the spatial distribution of observation counts from the Sentinel-1 and Sentinel-2 datasets over a ten-day period.

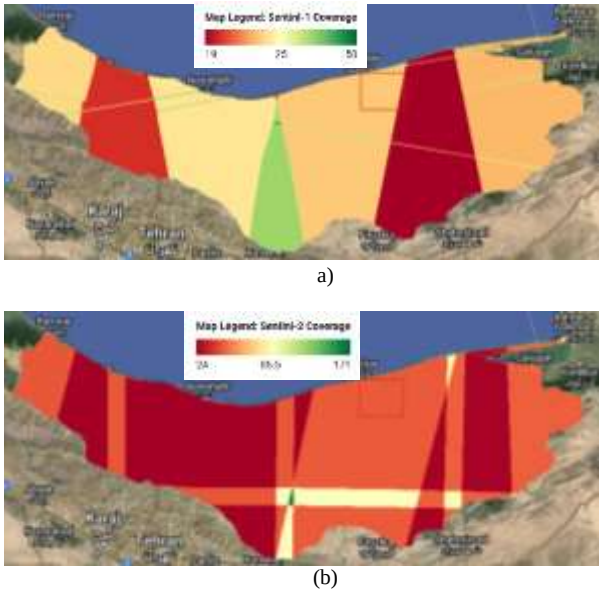

Figure 2. The number of valid satellite images during the rice planting season in Mazandaran province: a) based on Sentinel-1 images and b) based on Sentinel-2 images.

2.2.2. Sentinel-2

The Sentinel-2 mission is equipped with high-resolution, wide-swath multispectral imaging (MSI) capabilities. It has several objectives, including the analysis of vegetation, land use, water bodies, soil, and environmental conditions, as well as observations of inland water systems and coastal areas. The Sentinel-2A/B MSI Level-1C product provides top-of-atmosphere (TOA) reflectance data [19]. This dataset, which is used in the current study and available in GEE, includes 13 spectral bands covering visible, near-infrared, and shortwave infrared regions. The twin satellites revisit all continental land surfaces every five days, ensuring high temporal coverage.

2.2.3. Field Data and Dataset Labelling

Mazandaran Province, located in northern Iran, covers an area defined by the coordinates 52.36°N to 65.52°E and 71.36°N to 95.52°E (Figure 1). Ground truth data were collected from March to August over the years 2021 to 2023, encompassing 1166 rice samples and 5529 non-rice samples (e.g., forests, water bodies, urban areas). Approximately half—583 rice and 2764 non-rice— samples were utilized for training, while the remaining samples were reserved for testing. Sample data were gathered using two primary methods: manual collection through field visits and mobile GPS devices, and online collection via the GEE platform. Table 2 provides a summary of the field data. The agricultural lands in the region primarily consist of paddy fields and citrus orchards, while other types of agricultural areas are classified under the "farm" category. For training, approximately 30 percent of these agricultural areas were selected randomly, while the remaining 70 percent were reserved for testing.

Table 2. Number of ground truth data for different fields.

	Rice	Tree	Farm	Urban	Water
Polygon	56	40	18	25	20
Pixel	1166	621	148	2572	2188

3. Methodology

The approach employed in this study involves four main steps: (i) pre-processing of time-series images of Sentinel-1 and Sentinel-2 satellites; (ii) selecting appropriate indices and extracting time series indices; (iii) extract rice phenology curve from Sentinel-1 and Sentinel-2 images based on selected time series indices; (iv) crop mapping using rice phenology curve and correlation analysis.

3.1. Selection the appropriate indices for Sentinel-2 and Sentinel-1

Results of the classification will be more accurate when the classification features have better separability and stability. In other words, a suitable index to classify rice compared to other crops should possess the following features: It should exhibit a distinct pattern from other agricultural lands (or urban areas, trees and water) during the rice growing season. The more unique the selected index is for the paddy field, the easier and more accurate the rice mapping will be. It should be based on phenology and conditions of rice cultivation so that they have the same behavior for all paddy fields. It should also be less affected by environmental factors.

3.1.1. Selection the time series indices for Sentinel-2

After evaluating various indices extracted from Sentinel-2 satellite images, two indices NDVI [20] and LSWI [21] were selected, which calculated as follows:

$$NDVI = \frac{NIR-RED}{NIR+RED} \quad (1)$$

$$LSWI = \frac{NIR-SWIR}{NIR+SWIR} \quad (2)$$

where NIR, RED and SWIR are surface reflectance values in red, near infrared and shortwave infrared bands, respectively.

NDVI indicates the level of greenness. During the initial phases of rice growth, NDVI increases as the plant biomass expands. However, in the later stages, when the biomass stabilizes and the rice changes color, the index begins to decline. Essentially, the time-series pattern of the NDVI for rice follows a Gaussian curve. Since rice is cultivated in flooded conditions, and the LSWI is an index for detecting water presence, the LSWI will reach its highest value during the preparation and planting phases. As the plant biomass increases and rice grows, the observed water content from a satellite perspective diminishes, leading to a decline in this index. During the final growth stages, when the fields are dried for harvest, the LSWI value further decreases. To rephrase, during the various stages of rice growth, the LSWI demonstrates a consistently decreasing trend. Figure 3 illustrates the time-series curves of NDVI and LSWI for paddy fields after de-averaging. While NDVI is closely linked to rice phenology, LSWI is more influenced by the growing conditions of rice. Consequently, these indices are expected to exhibit similar behavior across all paddy fields within the study area.

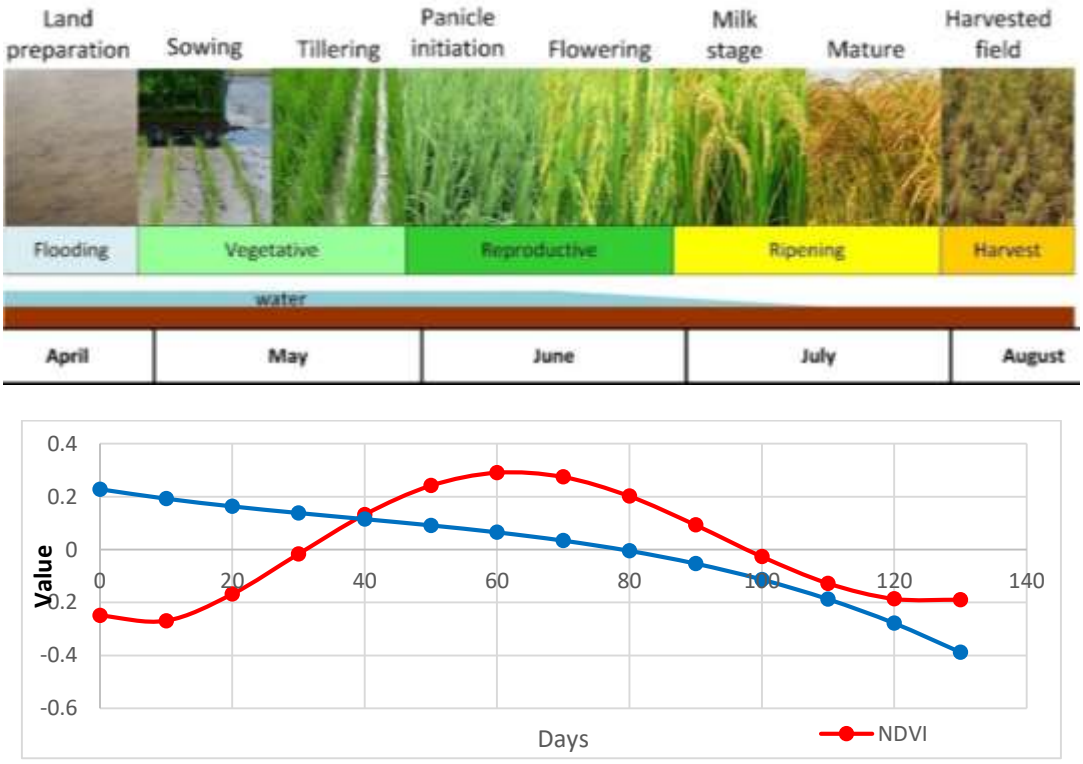

Figure 3. Changes of LSWI and NDVI indices during the growth stages of rice.

The time series profiles of LSWI and NDVI for paddy field after de-averaging are illustrated in Figure 4. NDVI index is related to rice phenology and LSWI is more dependent on rice growing conditions. Therefore, these indices are expected to behave almost the same for all paddy fields in this region.

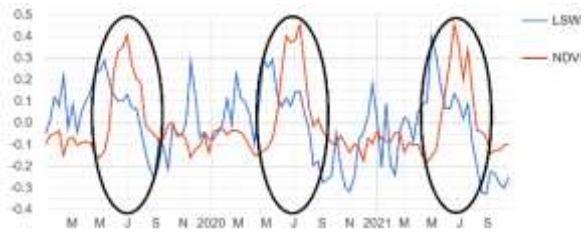

Figure 4. illustrate the time series profiles of NDVI and LSWI for paddy field.

3.1.2. Selection the time series indices for Sentinel-1

As we know, by increasing the number of independent and meaningful indices, the classification is done more accurately. For this purpose, Sentinel-1 satellite images were also used in the proposed method. In this way, the use of two satellites, in addition to increasing the number of independent indices, has the advantage that if the data of one satellite is not available at a certain time, the data of another can be used. Also, weather conditions have less effect on Sentinel-1 data. VV and VH bands of SAR images are available in the studied area. For this purpose, various indices were examined based on these two bands in order to choose the appropriate index. Table 1 shows the relationships of the indicators.

Table 3. Spectral indices used in the study and their formula.

Band Name	Formula	References
RVI (radar vegetation index)	$RVI = \frac{4VH}{VV+VH}$	[22]
RVI4S1(the Radar Vegetation Index for Sentinel-1)	$RVI4S1 = sqrt(\frac{VV}{VV+VH} \times \frac{4VH}{VV+VH})$	[26]
DPSVIc (Dual Polarization SAR Vegetation Index)	$DPSVIc = (\frac{VH}{VV}) \times (\frac{VH}{VV} + 3) / (1 + \frac{VH}{VV})^2$	[3]
CR (the cross-ratio)	$CR = \frac{VH}{VV}$	[27]

The values of these indices are plotted as a time series after pre-processing in Figure 5. As illustrated in Figure 5, these indices have similar behavior and only their amplitude is different from each other. Therefore, these indices are not independent of each other and only one of them can be used. Among these indices, the CR index was selected because in the proposed method, the magnitude of the indices is not important and only their time series behavior is important and on the other hand, this index has less computational processing. Figure 5 shows the time series graph of various index. In this figure, the NDVI index from Sentinel-2 is also plotted to check the simultaneity of the indices. As can be seen, this index has a different behavior for paddy fields than other fields during the rice cultivation period. Therefore, it can be used as an index for classification.

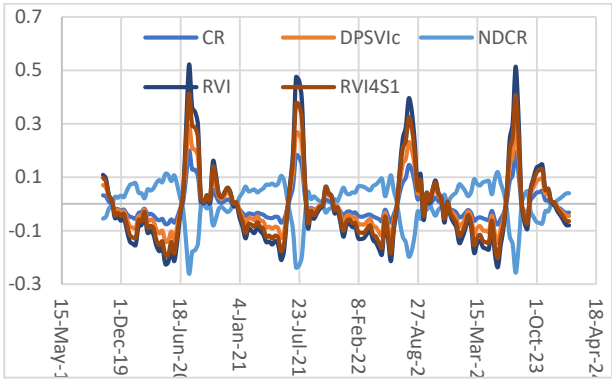

Figure 5. Curves of different time series indices from Sentinel-1 data.

3.2. Pre-processing and Extraction of Time Series Indices

Pre-processing of satellite images involves several key steps:

1- Eliminating cloudy pixels: Some pixels have low quality due to cloud cover and are unusable. They are removed from the input data to avoid incorrect results.

2-Ten-day quantization: the maximum visiting period of Sentinel-2 satellite is 5 days, and this is 6 days for Sentinel-1. To ensure consistency in the data and facilitate subsequent processing, the data from both satellites were quantized into ten-day periods. If the quantization period is too short, the quality of the data in each period and its accuracy will decrease. On the other hand, by choosing a long quantization period, the temporal information of the data is reduced. Therefore, the appropriate period (10 days) was selected. For further processing, we need to have exactly one value for each pixel in each 10-day interval. For this purpose, the time series images were averaged and as a result, one image was obtained for each ten-day period. For example, Figure 6 shows the count of valid Sentinel-2 scenes in the study area in the ten-day interval between 4/20/2023 and 8/24/2023. The number of images in each interval varies from zero to three depending on weather conditions and geographical location.

3- Interpolation of missing data: Interpolation was used to solve the problem of the lack of value of some pixels after quantization due to the removal of cloudy pixels. The interpolation method is explained in Table 4. In this table, the value of the pixel at time t is represented by $I(t)$.

4- Extracting time series indices.

Table 4. Interpolation procedure for cloudy pixels.

Interpolated pixel value at time t	Presence of pixel value at time t-1	Presence of pixel value at time t+1
$I(t) = \left[I(t-1) + I(t+1) \right] / 2$	Yes	Yes
$I(t) = I(t-1)$	Yes	No
$I(t) = I(t+1)$	No	Yes
$I(t) = 0$	No	No

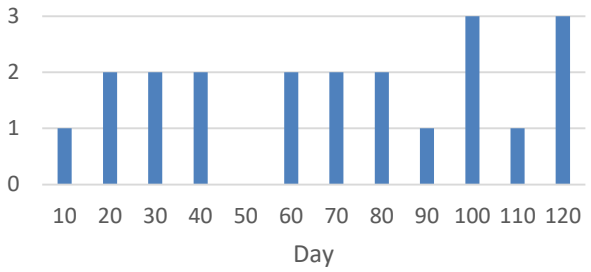

Figure 6. The count of valid Sentinel-2 scenes in the study area in the ten-day interval.

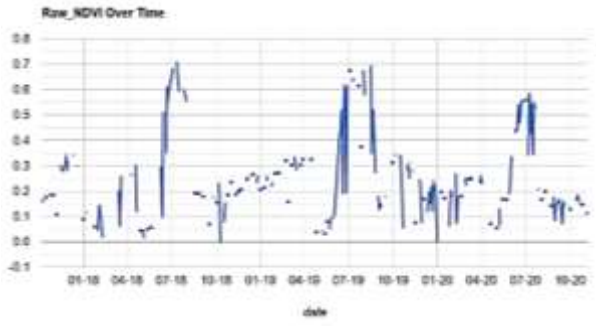

(a)

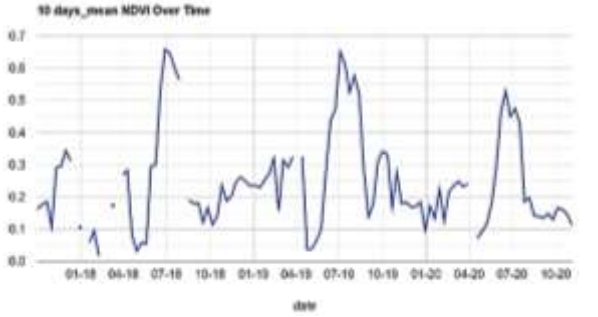

(b)

(c)

Figure 7. Time-series of NDVI: (a) After removing clouding pixels (b) After quantization and (c) After interpolation.

The results of each preprocessing step performed on a pixel of Sentinel-2 satellite images are presented in Figure 7. In Figure (7-a), the NDVI index is obtained from unprocessed images. As it is clear from this figure, the distance between the points is irregular and interrupted, which indicates that the number of scenes is not equal in different time intervals and the unavailability of the desired pixel data at some times. In Figure (7-b), NDVI is obtained from quantized images. In this figure, the distance between the points is equal, but there is still no data in some points. In Figure (7-c), NDVI is obtained from the interpolated images. In this figure, there is exactly one image for each 10-day period, And the indices extracted from these images can be used to continue the process.

3.3. Derivation of rice paddy phenology curves from Sentinel-1 and Sentinel-2 images

Since the proposed method relies on comparing each pixel's time series behavior with the rice phenology curve, accurately extracting this curve is essential for precise rice mapping. The process of extracting the rice paddy phenology curves for Sentinel-1 and Sentinel-2, using the selected time series indices, is explained as follows.

3.3.1. Derivation of rice paddy phenology curve from Sentinel-2 images

To extract the rice phenology curve, pre-processing steps as detailed in section (3.2) were implemented to the Sentinel-2 satellite images. NDVI and LSWI indices were then calculated for three consecutive years throughout the rice growing season and the average value across these three years was computed. Polynomial curve fitting functions were applied to the time series indices, with the polynomial degrees for fitting the NDVI and LSWI indices set to 6 and 3, respectively. The rice phenology curve for each index was derived using these polynomial functions. To prepare the phenology curves for use in the convolution operator, their average value was adjusted to zero (de-averaging) (Figure. 3).

3.3.2. Derivation of rice paddy phenology curve from Sentinel-1

First, the preprocessing of subsection (3.2) was performed on the Sentinel-1 images to have exactly one complete image every 10 days. Then, the CR index was extracted for three consecutive years during the rice cultivation period, and the 3-year average was calculated exactly in the same time period as the NDVI and LSWI curves. Finally, their average was set to zero. (Figure 8).

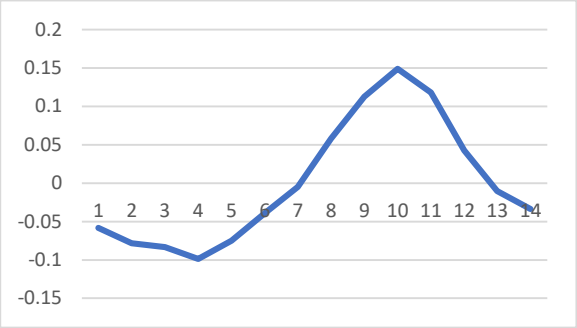

Figure 8. The CR index extracted as rice phenology curve from Sentinel-1.

4. Crop mapping using rice paddy phenology curve and correlation measurement

To map the rice crop, the similarity between each pixel's time series behavior and the rice phenology curve was analyzed. For this purpose, the maximum similarity between each pixel's behavior and the rice phenology curve was calculated for a specific period during the middle of the cultivation season and was used as a classifier feature for rice crop mapping. In the study area, in certain farms, rice is planted earlier due to consecutive rice cultivation, while in others, rice planting is delayed because of the successive cultivation with different crops. For this reason, the measurement interval of the maximum similarity value was considered large enough (50-days) to include all these fields. In this way, accelerating or delaying the cultivation and harvesting of rice has minimal impact on the results of the proposed method. The method consists of the following steps: (i) preprocessing satellite images and extracting time series indices; (ii) assessing the behavioral similarity of each pixel's time series indices with the improved rice phenology curves; and (iii) classification.

4.1. Obtaining behavioral similarity of time series indices of each pixel with improved rice phenology curves

The correlation operator was utilized to measure the similarity between the time series behavior of each pixel and the proposed rice phenology. Its implementation is as follows.

1- Subsection (3.2) pre-processing was done on Sentinel-1and Sentinel-2 images.

2- NDVI, LSWI and CR time series indices were extracted for each pixel.

3- For each time t, a window with the time interval [t-win_len/2 t+win_len/2] was created, where win_len is the length of the rice phenology curve.

4- To minimize the effect of low frequency changes in time series indices on the correlation results, the average value of each index in the window was calculated and then this average value was subtracted from the index values inside the window.

5- In each window, the dot product was performed between the rice phenology curves and the time series data of each index. The sum of the multiplication results was calculated and considered as the correlation value of the middle point of the window (t). By sweeping t in terms of time and calculating the correlation value for all times, the similarity of the phenological behavior of each pixel with rice phenology was obtained as a curve of time.

6- The maximum correlation value was calculated for each pixel over a period of 50-days. This period was almost in the middle of the rice cultivation period. The maximum correlation value that is limited in a certain time interval is used as the classification features in the next step.

$$Cor_X(t) = \sum_{i=-\lfloor W/2 \rfloor}^{\lfloor W/2 \rfloor} X(t+i).Ph_X(i) \qquad (3)$$

where $Cor_X(t)$ is the correlation value of index X at time t, W is the length of rice phenology curve (Ph_X), and $X(t)$ is the value of index at time t.

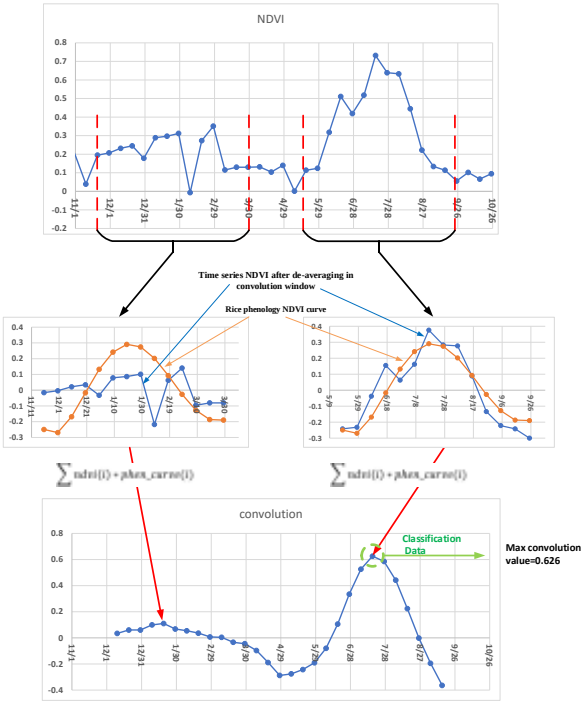

Figure 9. Correlation and feature extraction methods for classification on NDVI time series index.

In equation (1), steps 3 to 5 are expressed mathematically. Also, the correlation steps on the NDVI time series data of one pixel for two different times are drawn in Figure 9. This pixel is situated in the rice paddy field.

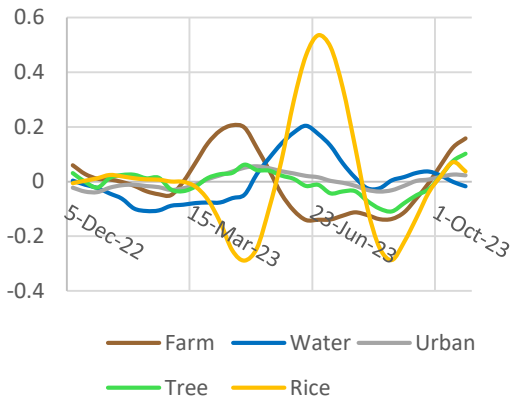

Figure 10. NDVI correlation results between the proposed rice phenology curve and the time series index of various fields over one year.

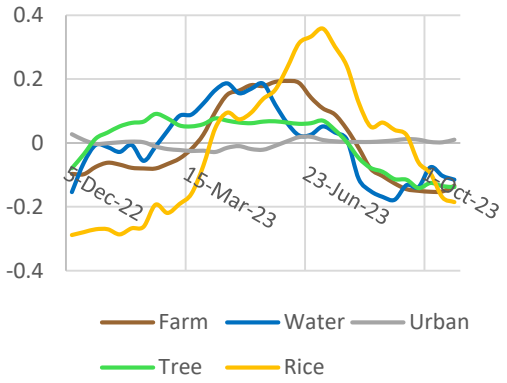

Figure 11. LSWI correlation results between the proposed rice phenology curve and the time series index of various fields over one year.

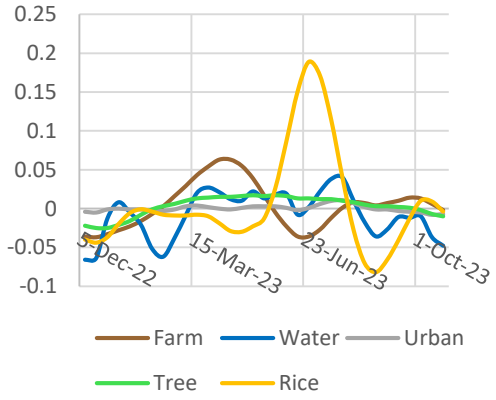

Figure 12. CR correlation results between the proposed rice phenology curve and the time series index of various fields over one year.

In Figures 10-12, the outputs of step 5 are shown. As evident from the figures, the maximum correlation value for paddy fields is significantly higher than that of other fields. In addition, for all three indices, this value happened simultaneously. Considering that the maximum value for paddy fields is significantly different from other crops, a good separation is expected from the classification.

The combined correlation of the indices is expressed in Eq. (2). And the result is shown in Figure 13.

$$ComCor_x(t) = \sum_{i=-\lfloor W/2 \rfloor}^{\lfloor W/2 \rfloor} [X_N(t+i).Ph_N(i) + X_L(t+i).Ph_L(i) + X_C(t+i).Ph_C(i)] \quad (4)$$

In this equation, X_N, X_L and X_C are NDVI, LSWI and CR time series respectively. Ph_N, Ph_L and Ph_C are the proposed rice phenology curves for NDVI, LSWI and CR.

Since the triple combined maximum correlation value is different from the sum of the 3 individual maximum correlation values, it is likely that using it alone as a classification feature (Figure 14) will give a different result than using the three individual correlations simultaneously. It will be tested in the next section.

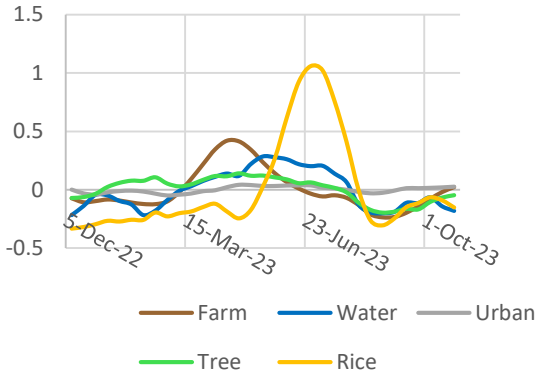

Figure 13. correlation results between the proposed rice phenology curve and the time series index of various fields over one year.

To determine the time frame for determining the maximum correlation, the maximum correlation value was drawn according to the time of occurrence of the maximum value (Figure 14). This figure is plotted for the NDVI index over a year (output of step 5) and each point represents the maximum correlation value of a random pixel from the field data. NDVI is stronger than the other two indices. It is clearly seen that the maximum value of correlation occurs for all pixels of paddy fields in a 50-day frame. The timing of this 50-day period is consistent with empirical knowledge about rice. For rice crop mapping, the maximum value of correlation was calculated in this time frame, which is slightly different from the maximum value in the whole year.

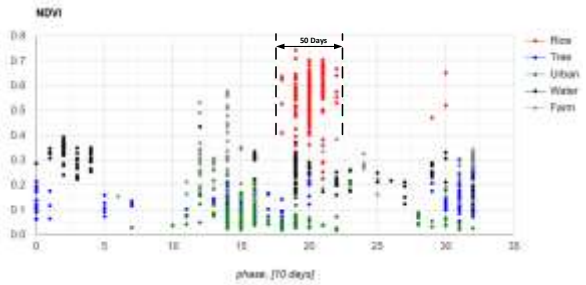

Figure 14. Maximum correlation value of random pixels from field data during one year.

4.2. Classification

In the previous section, correlation was calculated to evaluate the behavioral similarity of each pixel with paddy fields. Subsequently, the maximum correlation value for each index was identified within a specific time period. The maximum value of correlations was utilized as input features of the classifier. The classification was performed using an SVM-RBF classifier.

The flowchart of paddy field mapping is shown in Figure 15.

5. Results

In the previous section, the pre-processing performed on Sentinel- 1and Sentinel-2 images to produce 10-day quantized images was described. Subsequently, the time series indices of NDVI, LSWI and CR were obtained. To extract classification features, the similarity of each time series index with rice phenology curve was calculated. Correlation operator was used to measure similarity. The maximum correlation value in a period of 50-days in the middle of the rice cultivation period was used as the classifier feature. Figures 16-18 show the maximum correlation value of each index for different lands. In these figures, each point represents a randomly selected pixel from the test data set. These figures show that the NDVI index has a better separation compared to the LSWI and CR indices. Since the LSWI and CR indices are separable to some extent, it is obvious that the combined use of the indices will have better results. Figure 19 illustrates the result of the combined correlation of three indices. As it is clear from the figure, the maximum similarity of paddy fields to the phenology curve of rice is much higher than other fields and it happens in a certain period of time. Therefore, these features are completely separable with a simple classification.

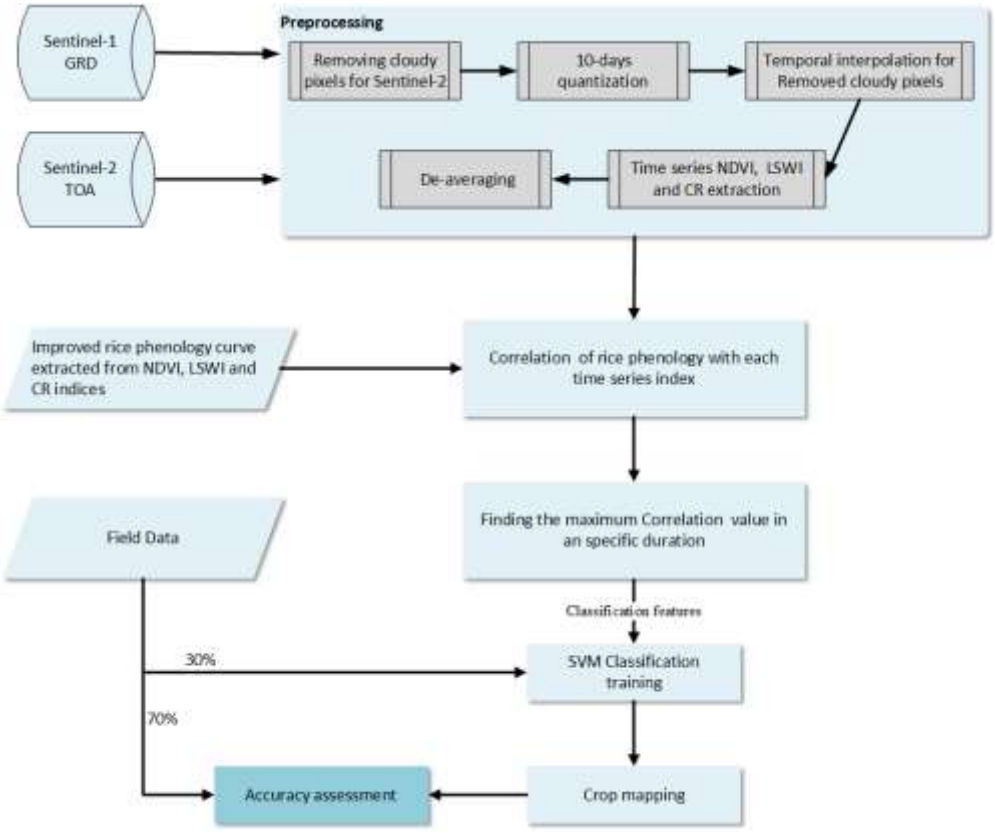

Figure 15. Methodological workflow of paddy field mapping.

Figures 16 to 19 show that for most fields, the maximum value occurs in the middle of the rice cultivation period, and the number of fields in which cultivation is done earlier or later is less.

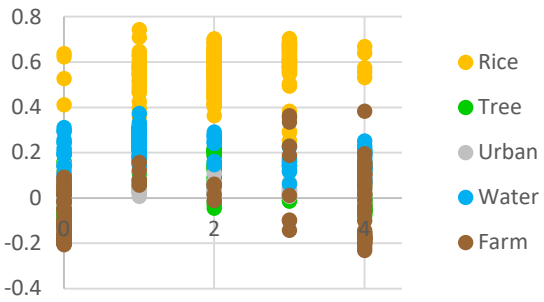

Figure 16. Maximum correlation value related to NDVI index for different lands.

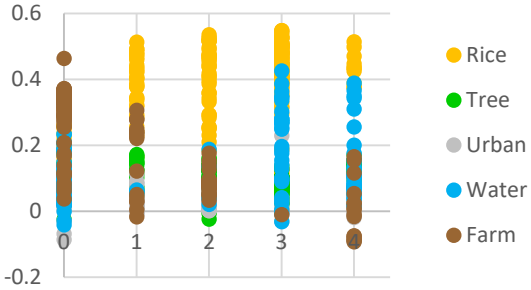

Figure 17. Maximum correlation value related to LSWI index for different lands.

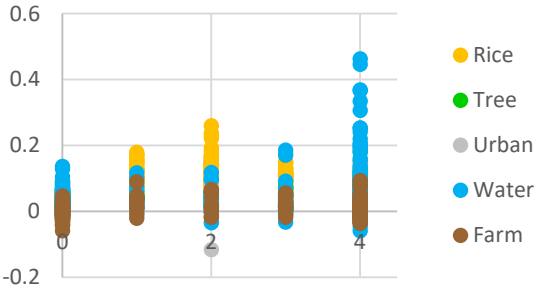

Figure 18. Maximum correlation value related to CR index for different lands.

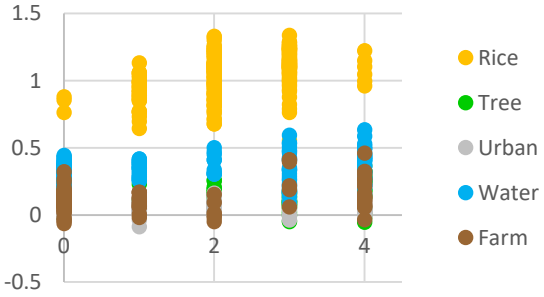

Figure 19. The maximum value of the combined correlation of three indices NDVI, LSWI and CR for different lands.

The classification results using SVM-RBF classifier are presented in Table 5. The values of rice crop mapping are given based on the maximum correlation value of each index, the combined correlation value, and the simultaneous use of the correlation values of three indices as classification input features.

Table 5. Overall accuracy evaluation results based on different features in 2023.

Feature Vector	Train	Test
NDVI	0.990	0.994
LSWI	0.907	0.923
CR	0.885	0.864
Combined Correlation	0.994	0.993
NDVI, LSWI, CR	0.997	0.999

Table 5 shows that the classification based on the simultaneous use of the separate correlation of three indicators is slightly better than the classification based on the combined correlation of the three indicators. The remarkable thing about this method is that the classification was done only based on the maximum similarity. Additionally, the timing of the occurrence of this maximum similarity was not important and on the other hand, the maximum amount has been obtained in a wider time period than the rice cultivation period. Consequently, delays or accelerations in rice cultivation or harvesting have minimal impact on the classification results.

Figure 20 shows the mapping of paddy fields using the NDVI index. Figure (20-a) shows a part of the studied area. The result of the correlation between the NDVI index and the NDVI phenology curve of rice is shown in Figure (20-b). This image is based on the maximum correlation value over a year. It is in gray scale. In other words, the brightness of a pixel indicates how closely its time series behavior aligns with rice phenology. Therefore, the bright pixels belong to the paddy fields. Figure (20-d) shows the classification based on the image (20-b), that is, the classification based on the maximum correlation value in a year. This image clearly shows the effective classification. But in the center of this landscape is a shallow farm lake that is partially dried up and overgrown with weeds (marked with a yellow box). It seems that the phenology of these weeds for NDVI is almost the same as that of rice, identified in image (20-b) and incorrectly identified as paddy in image (20-d). In figure (20-c), the time to extract the maximum correlation value is limited to a period of 50-days in the middle of the rice cultivation season. By comparing figure (20-c) with figure (20-b), we find that by limiting the maximum correlation extraction time, the difference between paddy fields and other fields increases. Also, this value is greatly reduced (pixels become darker) for weeds

inside the shallow farm lake (yellow box). Also, this value is greatly reduced (pixels darken) for the weeds inside the shallow farm lake (yellow box) because the phenological changes of these weeds and paddy fields do not occur simultaneously and occur in different seasons of the year. In figure (20-e) the classification based on the values of figure (20-c) is shown. As expected, the classification in this case was much more accurate than in Figure (20-d), and the fields inside the yellow box (weeds) were correctly classified as non-paddy fields.

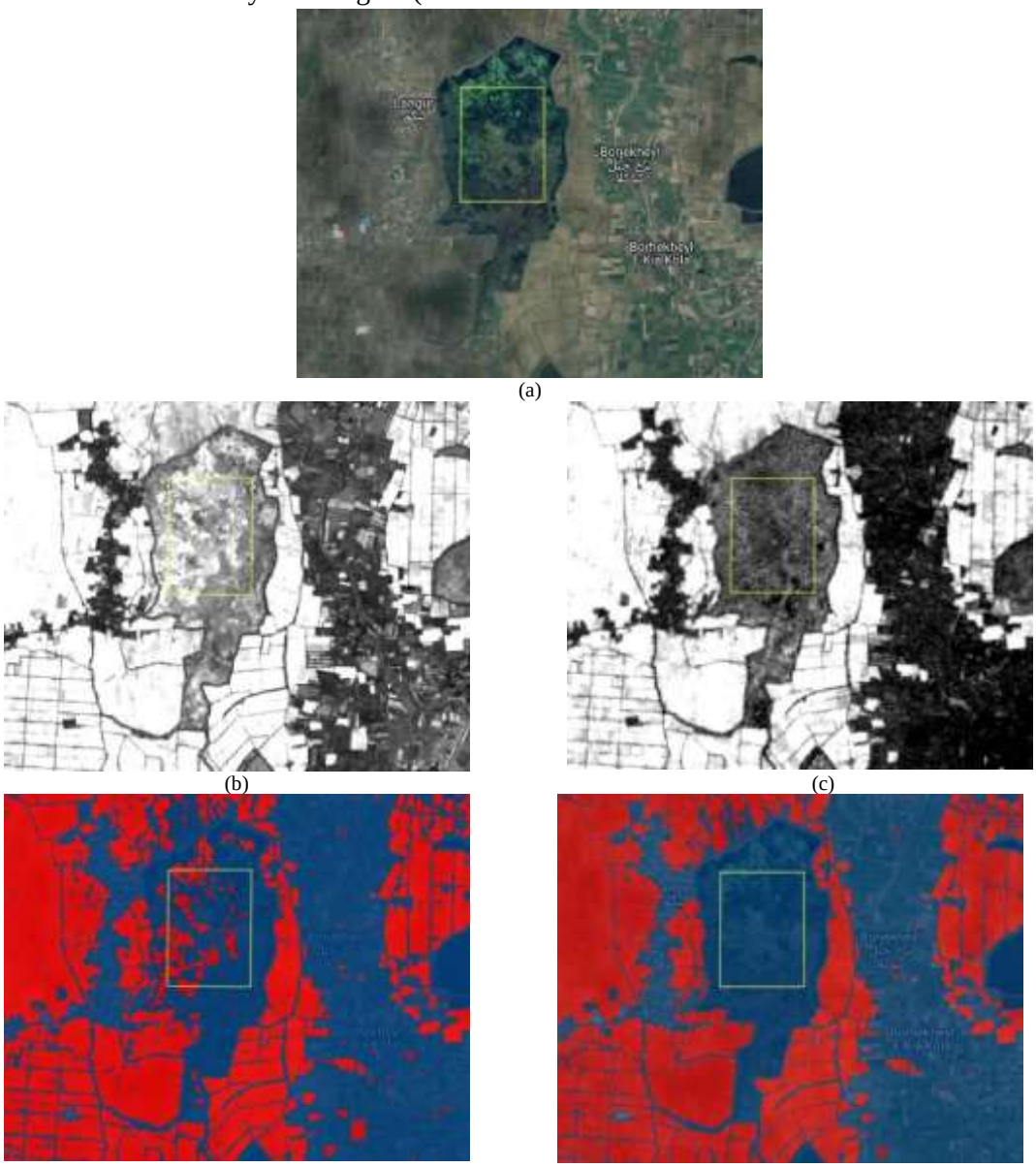

Figure 20: mapping of paddy fields using the NDVI index: (a) the part of the studied area; Illustration of (b) the maximum correlation value over a year, and (c) the maximum correlation value limited to a period of 50-days; Crop mapping results based on (d) image b, and (e) image c, with rice marked in red.

The maximum value of the combined correlation of three indices NDVI, LSWI and CR with rice phenology curves is shown in Figure (21-b). This image, like figure (20-b), is obtained from the maximum correlation value over a year. By comparing Figures (21-b) and (20-b), we find that the use of combined correlation provides better separation between paddy fields and other fields (higher color difference). More importantly, in this image, the pixels corresponding to weeds in the shallow farm lake are paler than in Fig. (20-b). The reason is that although for the NDVI index, the phenology of these weeds is similar to that of the paddy field, it is different for the LSWI and CR indices. As a result, the combined use of three indices has reduced the similarity of pixels related to weeds and paddy fields. Figure (20-c) is based on the maximum correlation (similarity) in the limited period of 50-days. Figures (21-d) and (21-

e) of paddy field mapping are based on the values of figures (21-b) and (21-c) respectively.

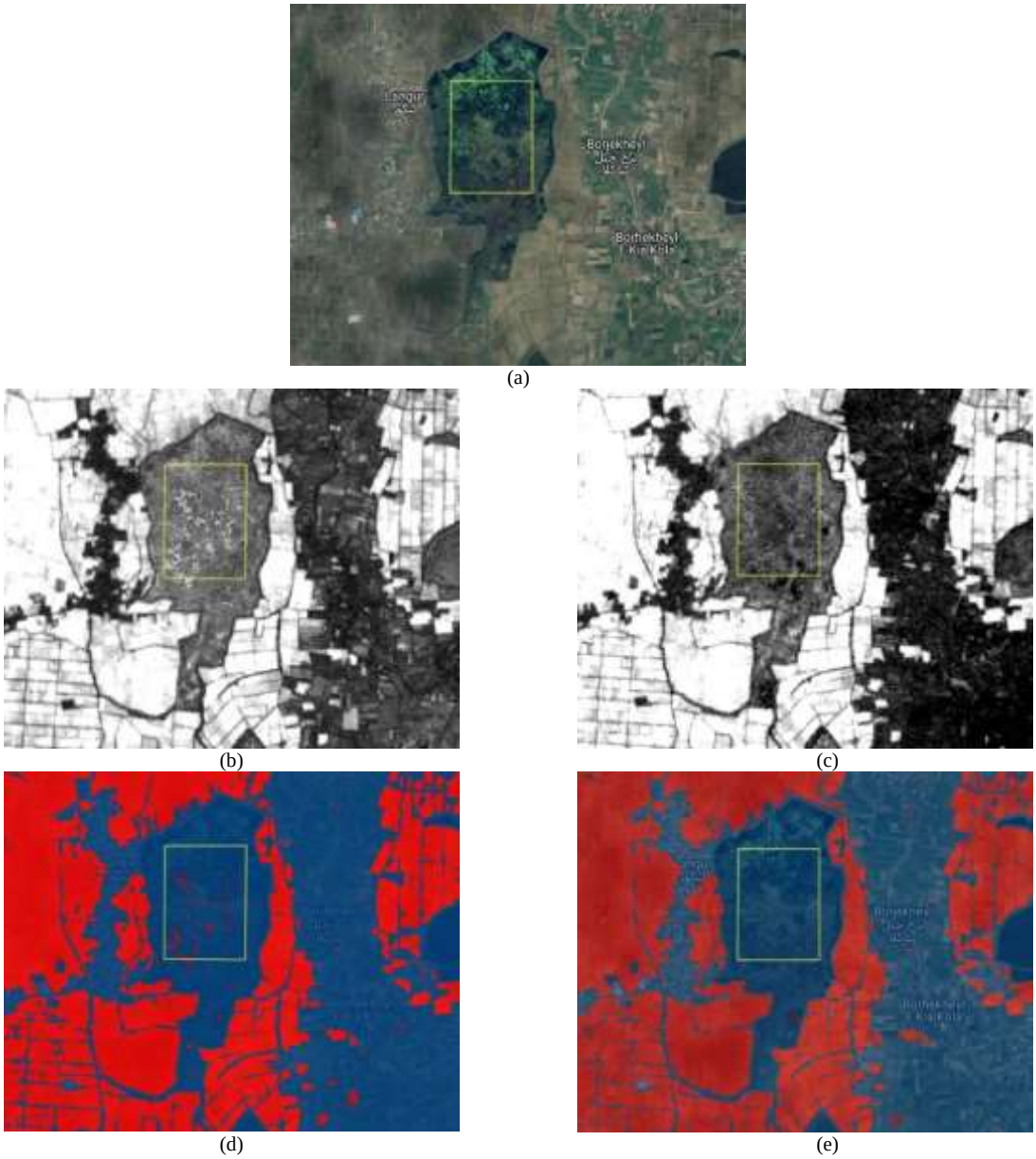

Figure 21: mapping of paddy fields using combined correlation of three indices NDVI, LSWI and CR: (a) the part of the studied area; Illustration of (b) the maximum correlation value over a year, and (c) the maximum correlation value limited to a period of 50 days; Crop mapping results based on (d) image b, and (e) image c, with rice marked in red.

For a better visual representation of the classification accuracy, a portion of the study area with fragmented and relatively small fields is presented in Figure (22-a). Figure (22-b) is a manual mapping of the paddy field with visual inspection. In Figure (22-c), the mapping of paddy fields was done based on the simultaneous use of the separate correlation of three indices as classification features. As it is clear from the figure, the fields are small. According to the ratio of the dimensions of the land to the dimensions of the pixels of Sentinel-1 and Sentinel-2 images, a large percentage of the pixels of the satellite images are located on the border of two types of land and are a combination of them. This makes it difficult to distinguish between lands. However, in the proposed method, good mapping was achieved.

(a)

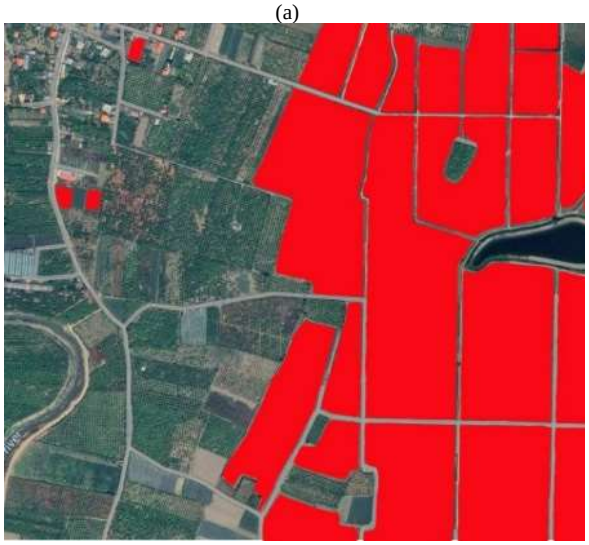

(b)

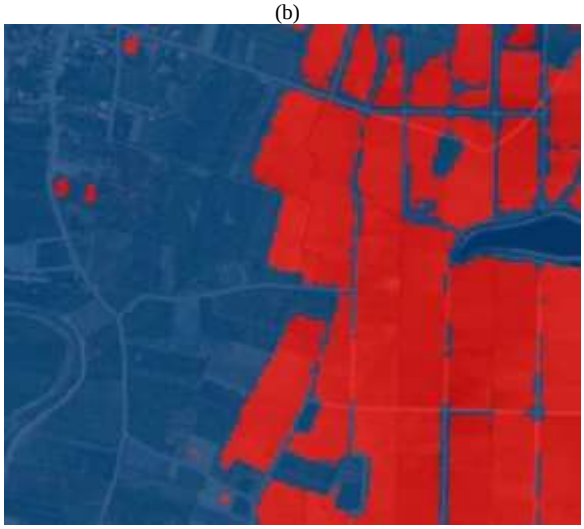

(c)

Figure 22. Visualization of paddy field mapping based on the simultaneous use of separate correlations of three indices: (a) a visualized portion of the study area; (b) ground truth data with rice highlighted in red; (c) crop mapping results with rice highlighted in red.

In addition, the edges of image (22-c) are not as smooth as image (22-b), because image (22-b) is created from high-resolution images, but images of classified regions (red color) are derived from the images of Sentinel-1 and Sentinel-2 satellites, which have a lower resolution.

If satellite images with higher resolution are used instead of Sentinel-1 and Sentinel-2 images, the edge of the classified images will be smoother and the interference of the fields in one pixel will be reduced and better classification will be done.

6. Discussion

Numerous studies have been conducted on crop mapping using phenology. Most of these studies fall into two main groups: A) Approaches based on thresholds, and B) Approaches based on Machine learning. In the following, we will examine each method and their problems.

Thresholding-based methods: In this method, phenology parameters such as Start of Season (SOS), End of Season (EOS), or Growing Season Length (GSL) are derived by applying thresholds to indices like NDVI, LSWI from Sentinel-2, or band values such as HV and VV from Sentinel-1. Crop mapping is then performed based on these parameters. For example, [22] first extracted the NDVI, REP, and NDRI parameters during the middle of the growing season from Sentinel-2 imagery. The ΔNDVI parameter was calculated as the difference between the NDVI values at the midpoint and the end of the growing season. Then by thresholding these parameters, crop mapping was done. In another study by [23], five parameters of Flooding Frequency (FF), Cropping Intensity (CI), Cropping Diversity (CD) and coefficient of variation (CV) were extracted from the VH band values and EVI and LSWI indices. The relationship between LSWI and EVI was used to obtain FF, and when LSWI was greater than EVI, it was considered as the start of flood time. To obtain the CI parameter, the number of local maximum occurrences of the EVI index in one year was counted. To obtain the CD parameter, each time the EVI reached a local maximum, the difference between the maximum and minimum EVI values was calculated. Also, the difference ratio of these values was used to obtain crop diversity (CD). The CV parameter is the value of the covariance in the EVI index. crop classification was done by thresholding these parameters.

In general, threshold-based methods are extremely dependent on the index values at specific times. If the value of these indices changes due to reasons such as low quality of images due to cloudiness or other factors, the extracted phenology parameters will not be accurate [16]. It is possible that due to weather conditions, the index value for weeds is within the range of the crop index, which causes

errors in the final result. Also, in areas where due to successive cultivation, it is possible to plant rice earlier or later in some lands. Therefore, in these lands, the occurrence time of phenology parameters such as SOS and EOS are shifted, which has a negative result on mapping using these methods. Another limitation of this method is the presence of waterside pixels. If the boundary of water bodies is moved between before and after harvesting due to factors such as temperature and rainfall, the index values of the water edge pixels will change, which is called the water edge effect [24].

Machine learning based techniques: Different machine learning algorithms are used for product mapping [25], [26] and [27]. Many studies demonstrate that the presence of redundant and dependent features, in addition to increasing the computational cost in various machine learning techniques, reduces accuracy. Consequently, it is proposed to select a set of independent and impactful features to enhance the performance of the classifier. The features used in machine learning are usually divided into two general categories: 1) Features that are based on the value of indices such as NDVI, LSWI, etc. or the value of bands such as VH and VV at certain times; 2) Features based on phenology parameters such as EOS, SOS, etc. For example, in [28], the EVI2 index [29] was extracted from Sentinel-2 images. The ratio of EVI2 changes was calculated for different times and then by thresholding the ratio of changes in EVI2, SOS and EOS values for threshold values of 10, 50 and 90% were obtained. Finally, with the help of the RF classifier, the lands were divided into two categories: crop land and non-crop land. As mentioned earlier, many factors affect these Features. Feature inaccuracy negatively affects the output of machine learning-based classification.

In the studied area, due to the multi-cultivation of the land, the rice planting and harvesting time may change a little. Also, in this region, by moving away from the sea and moving towards the foothills, due to the decrease in temperature, rice planting takes place later and the rice cultivation period increases. Another characteristic of this region is the smallness of the agricultural land and the diversity of its cultivation, and it is possible to cultivate and harvest different crops at the same time and due to the cloudiness of the area, satellite images may not be available at different times. According to the conditions of the region, most of the methods mentioned above are not very effective in the region. Therefore, in the proposed method, an attempt was made to present a method that is less affected by environmental and atmospheric changes or human activities. In the proposed method, the value of indices at a specific time is not used for classification. Instead, the time series behavior of each pixel indices was examined in the entire cultivation period, and the similarity of the time series behavior of each pixel indices and rice phenology curves were used for classification. In this way, unwanted changes in the value of an index at some times or the unavailability of an index at different times do not have much effect on rice mapping. In other words, this method is resistant to environmental changes. In this method, the time period for determining the maximum correlation (similarity of the phenology of each pixel with rice) is 50 days. On the other hand, in the studied area, due to the weather conditions, the time range of rice transplanting is limited and it is not possible to change it to more than 50 days. In other words, acceleration or delay in planting rice does not have much effect on the classification result of the proposed method. The use of three independent indices, NDVI, LSWI and CR, as well as the use of correlation in the entire cultivation period, have created features with high separation and resistance.

7. Conclusion

The lands in the study area, are fragmented, small and interspersed with other uses/covers. There are many cloudy days and so field data is limited. In this paper, a phenology-based method is presented to address these challenges. First, a series of pre-processing are done on the images of the Sentinel-1 and Sentinel-2 satellites. Pixels with inappropriate data are removed, 10-day quantization is performed, and pixels with missing values are interpolated based on the time series data.

CR index from Sentinel-1 and two independent indices NDVI and LSWI are calculated from Sentinel-2 data. The indices are chosen in such a way that the time series behavior of each index for paddy field is different from the other fields and at the same time is constant for all paddy fields. To classify each pixel, the time series behavior of each index of that pixel is compared with the phenology curve of the paddy field. Correlation operator is used to get their similarity. The highest value of correlation occurs when the rice phenology curve matches the time series behavior of the pixel. It is clear that the maximum correlation time for a pixel of paddy field is in the middle of the cultivation period. A 50-day interval in the middle of the cultivation period is chosen to determine the maximum correlation of each pixel so that all the

fields in which rice transplanting is done earlier or later are included in this interval. On the other hand, the shortness of this interval means that for other products, the time of maximum correlation is more likely to be outside this range (Of course, the maximum correlation value for paddy fields is always higher than other lands). In this way, the difference between paddy fields and other lands increases. The maximum correlation value of three indices CR, NDVI and LSWI is used as classification feature. Considering that the correlation result has a good separation capability and the three indices are independent of each other, the classification is easy and can be done by different machine learning algorithms. In this study, classification is performed using SVM-RBF. This method demonstrates high robustness against environmental factors, and the experimental results validate its performance, achieving an overall accuracy of 99%. All processing is conducted on the GEE cloud platform.

However, if consecutive satellite images are unavailable during the rice growing season due to cloudy conditions, the interpolation accuracy will decrease, ultimately affecting the reliability of crop mapping results. Furthermore, as the ratio of land dimensions to pixel dimensions decreases, the proportion of border pixels between two land types relative to the number of interior pixels increases. Border pixels may contain mixed crop types, but in crop mapping, they are assigned to a single category, reducing mapping accuracy. To mitigate this, higher-resolution satellite images can be used to improve accuracy, or object-based processing can be applied to high-quality RGB images to detect boundaries between different land types. Subsequently, based on the classification results of the proposed method, the crop type of each land plot within the identified boundaries can be determined.

To increase the accuracy of mapping, object-based processing can be performed on high-quality images to detect the boundary between different lands. Then, based on the classification results of the proposed method, the type of each piece of land enclosed between the borders can be determined.

Funding This research is funded by Babol Noshirvani University of Technology through Grant program No. BNUT/389079/ 1403-1.

References

[1] P. A. Seck, A. Diagne, S. Mohanty, and M. C. Wopereis, "Crops that feed the world 7: Rice," *Food security*, vol. 4, pp. 7-24, 2012.

[2] J. Dong, X. Xiao, M. A. Menarguez, G. Zhang, Y. Qin, D. Thau, C. Biradar, and B. Moore III, "Mapping paddy rice planting area in northeastern Asia with Landsat 8 images, phenology-based algorithm and Google Earth Engine," *Remote Sensing of Environment*, vol. 185, pp. 142-154, 2016

[3] N. Bhogapurapu, S. Dey, D. Mandal, A. Bhattacharya, L. Karthikeyan, H. McNairn, and Y. S. Rao, "Soil moisture retrieval over croplands using dual-pol L-band GRD SAR data," *Remote Sensing of Environment*, vol. 271, p. 112900, 2022.

[4] Y. Jiang, H. Qian, S. Huang, X. Zhang, L. Wang, L. Zhang, M. Shen, X. Xiao, F. Chen, H. Zhang, and C. Lu, "Acclimation of methane emissions from rice paddy fields to straw addition," *Science Advances*, vol. 5, no. 1, p. eaau9038, 2019.

[5] M. Gilbert, N. Golding, H. Zhou, G. W. Wint, T. P. Robinson, A. J. Tatem, S. Lai, S. Zhou, H. Jiang, D. Guo, and Z. Huang, "Predicting the risk of avian influenza A H7N9 infection in live-poultry markets across Asia," *Nature Communications*, vol. 5, no. 1, p. 4116, 2014.

[6] M. Zhang, H. Lin, G. Wang, H. Sun, and J. Fu, "Mapping paddy rice using a convolutional neural network (CNN) with Landsat 8 datasets in the Dongting Lake Area, China," *Remote Sensing*, vol. 10, no. 11, p. 1840, 2018.

[7] W. Zhang, H. Liu, W. Wu, L. Zhan, and J. Wei, "Mapping rice paddy based on machine learning with Sentinel-2 multi-temporal data: Model comparison and transferability," *Remote Sensing*, vol. 12, no. 10, p. 1620, 2020.

[8] H. C. de Castro Filho, O. A. de Carvalho Júnior, O. L. F. de Carvalho, P. P. de Bem, R. dos S. de Moura, A. O. de Albuquerque, C. R. Silva, P. H. G. Ferreira, R. F. Guimarães, and R. A. T. Gomes, "Rice crop detection using LSTM, Bi-LSTM, and machine learning models from Sentinel-1 time series," *Remote Sensing*, vol. 12, no. 16, p. 2655, 2020.

[9] X. Shi, Z. Chen, H. Wang, D.-Y. Yeung, W.-K. Wong, and W.-c. Woo, "Convolutional LSTM network: A machine learning approach for precipitation nowcasting," Advances in neural information processing systems, vol. 28, 2015.

[10] M. Rußwurm and M. Körner, "Convolutional LSTMs for cloud-robust segmentation of remote sensing imagery," arXiv preprint arXiv:1811.02471, 2018.

[11] G. Tian, H. Li, Q. Jiang, B. Qiao, N. Li, Z. Guo, J. Zhao, and H. Yang, "An automatic method for rice mapping based on phenological features with Sentinel-1 time-series images," Remote Sensing, vol. 15, no. 11, p. 2785, 2023.

[12] S. Park, J. Im, S. Park, C. Yoo, H. Han, and J. Rhee, "Classification and mapping of paddy rice by combining

Landsat and SAR time series data," *Remote Sensing*, vol. 10, no. 3, p. 447, 2018.

[13] Y. He, J. Dong, X. Liao, L. Sun, Z. Wang, N. You, Z. Li, and P. Fu, "Examining rice distribution and cropping intensity in a mixed single-and double-cropping region in South China using all available Sentinel 1/2 images," *International Journal of Applied Earth Observation and Geoinformation*, vol. 101, p. 102351, 2021.

[14] Z. He, S. Li, Y. Wang, L. Dai, and S. Lin, "Monitoring rice phenology based on backscattering characteristics of multi-temporal RADARSAT-2 datasets," *Remote Sensing*, vol. 10, no. 2, p. 340, 2018.

[15] J. Li and D. P. Roy, "A global analysis of Sentinel-2A, Sentinel-2B and Landsat-8 data revisit intervals and implications for terrestrial monitoring," *Remote Sensing*, vol. 9, no. 9, p. 902, 2017.

[16] L. Liu, X. Xiao, Y. Qin, J. Wang, X. Xu, Y. Hu, and Z. Qiao, "Mapping cropping intensity in China using time series Landsat and Sentinel-2 images and Google Earth Engine," Remote Sensing of Environment, vol. 239, p. 111624, 2020.

[17] L. Pan, H. Xia, X. Zhao, Y. Guo, and Y. Qin, "Mapping winter crops using a phenology algorithm, time-series Sentinel-2 and Landsat-7/8 images, and Google Earth Engine," *Remote sensing*, vol. 13, no. 13, p. 2510, 2021.

[18] F. Namazi, M. Ezoji, and E. G. Parmehr, "Paddy Rice mapping in fragmented lands by improved phenology curve and correlation measurements on Sentinel-2 imagery in Google earth engine," *Environmental Monitoring and Assessment*, vol. 195, no. 10, p. 1220, 2023.

[19] F. Gascon, C. Bouzinac, O. Thépaut, M. Jung, B. Francesconi, J. Louis, V. Lonjou, B. Lafrance, S. Massera, A. Gaudel-Vacaresse, and F. Languille, "Copernicus Sentinel-2A calibration and products validation status," *Remote Sensing*, vol. 9, no. 6, p. 584, 2017.

[20] X. Xiao, S. Boles, J. Liu, D. Zhuang, S. Frolking, C. Li, W. Salas, and B. Moore III, "Mapping paddy rice agriculture in southern China using multi-temporal MODIS images," *Remote Sensing of Environment*, vol. 95, no. 4, pp. 480-492, 2005.

[21] C. J. Tucker, "Red and photographic infrared linear combinations for monitoring vegetation," *Remote sensing of Environment*, vol. 8, no. 2, pp. 127-150, 1979.

[22] Y. Kim and J. J. Van Zyl, "A time-series approach to estimate soil moisture using polarimetric radar data," IEEE Transactions on Geoscience and Remote Sensing, vol. 47, no. 8, pp. 2519-2527, 2009.

[23] Y. Jiang, Z. Lu, S. Li, Y. Lei, Q. Chu, X. Yin, and F. Chen,"Large-scale and high-resolution crop mapping in China using Sentinel-2 satellite imagery," *Agriculture*, vol. 10, no. 10, p. 433, 2020.

[24] Y. Liu, Q. Yu, Q. Zhou, C. Wang, S. D. Bellingrath-Kimura, and W. Wu, "Mapping the complex crop rotation systems in Southern China considering cropping intensity, crop diversity, and their seasonal dynamics," *IEEE Journal of Selected Topics in Applied Earth Observations and Remote Sensing*, vol. 15, pp. 9584-9598, 2022.

[25] J. Tian, Y. Tian, Y. Cao, W. Wan, and K. Liu, "Research on Rice fields extraction by NDVI difference method based on sentinel data," *Sensors*, vol. 23, no. 13, p. 5876, 2023.

[26] R. Zhao, Y. Li, and M. Ma, "Mapping paddy rice with satellite remote sensing: A review," Sustainability, vol. 13, no. 2, p. 503, 2021.

[27] C. Huang, S. You, A. Liu, P. Li, J. Zhang, and J. Deng, "High-Resolution National-Scale Mapping of Paddy Rice Based on Sentinel-1/2 Data," *Remote Sensing*, vol. 15, no. 16, p. 4055, 2023.

[28] P. Wei, H. Ye, S. Qiao, R. Liu, C. Nie, B. Zhang, L. Song, and S. Huang, "Early crop mapping based on Sentinel-2 time-series data and the random forest algorithm," *Remote Sensing*, vol. 15, no. 13, p. 3212, 2023.

[29] A. Htitiou, A. Boudhar, A. Chehbouni, and T. Benabdelouahab, "National-scale cropland mapping based on phenological metrics, environmental covariates, and machine learning on Google Earth Engine," *Remote Sensing*, vol. 13, no. 21, p. 4378, 2021.

[30] Z. Jiang, A. R. Huete, K. Didan, and T. Miura, "Development of a two-band enhanced vegetation index without a blue band," *Remote Sensing of Environment*, vol. 112, no. 10, pp. 3833-3845, 2008.

نقشه برداری برنج بر پایه فنولوژی با تجزیه و تحلیل همبستگی بر روی تصاویرسنتینل-۱ و ۲ در زمین های تکه تکه شده با استفاده از بستر GEE

فاطمه نمازی[۱]، مهدی ازوجی[۱*] و عبادت قنبری پرمهر[۲]

[۱] دانشکده مهندسی برق و کامپیوتر، دانشگاه صنعتی نوشیروانی بابل، بابل، ایران.

[۲] گروه نقشه‌برداری، دانشکده مهندسی عمران، دانشگاه صنعتی نوشیروانی بابل، بابل، ایران.

ارسال ۲۰۲۴/۱۲/۰۸؛ بازنگری ۲۰۲۵/۰۱/۳۰؛ پذیرش ۲۰۲۵/۰۳/۰۶

چکیده:

پراکندگی شالیزارها و همجواری آن با محصولات دیگر در شمال ایران، نقشه‌برداری محصول با روش‌های سنجش از دور را با چالش‌های متعددی روبه‌رو می‌کند. همچنین، شـرایط آب و هوای ابری منطقه، کیفیت تصـاویر ماهواره‌ای را کاهش می‌دهد یا آن‌ها را غیرقابل اسـتفاده می‌کند و فرآیند پایش را دشوارتر می‌سازد. در این مقاله، روشی برای رفع چالش‌های موجود در نقشه‌برداری شالیزار بر پایه فنولوژی برنج ارائه می‌دهد. در این روش، منحنی‌های فنولوژی برنج از داده‌های سری زمانی ماهواره‌های سنتیل-۱ و سنتینل-۲ استخراج می‌شود. این منحنی‌ها بر اساس شاخص نسبت متقاطع (CR) از سنتیل-۱ و شاخص‌های NDVI (شاخص به‌هنجار شده تفاوت پو شش گیاهی) و LSWI (شاخص سطح آب زمین) از سنتیل-۲ ایجاد شده ا ست. برخلاف بیشتر روش‌های موجود، که بر تحلیل شاخص‌ها در زمان‌های مشخصی تمرکز دارند، روش پیشنهادی به بررسی رفتار سری زمانی شاخص‌های هر پیکسل در طول دوره کشت می‌پردازد. این رویکرد، تأثیر منفی پوشش ابری بر روی دقت نقشه‌برداری محصول را به‌طور چشم‌گیری کاهش می‌دهد. برای نقشه‌برداری محصول، ابتدا همبستگی شاخص‌های سری زمانی هر پیکسل با منحنی‌های فنولوژی برنج محاسبه شده و در یک بازه‌ی ۵۰ روزه در اواسط دوره کشت برنج، مقادیر بیشینه همبستگی هر سه شاخص به‌دست آمده و به عنوان ویژگی‌هایی در طبقه‌بندی به‌کار گرفته شده است. ارزیابی کمی و کیفی کارایی روش پیشـــنهادی، دقت بالای آن را تأیید کرده، به‌گونه‌ای که دقت کلی این روش در منطقه مورد مطالعه در شـــمال ایران برابر با ۹۹.۷ درصد به دست آمده است. همه پیاده‌سازی‌ها و فرآیندها بر بستر Google Earth Engine (GEE) اجرا شده است.

کلمات کلیدی: تخمین سطح زیر کشت برنج، فنولوژی برنج، سنتینل-۱ و ۲، زمین های کشاورزی تکه تکه، همبستگی، GEE.